Journal of Sound and Vibration (1999) **228**(1), 177–197
Article No. jsvi.1999.2408, available online at http://www.idealibrary.com on IDEAL®

THE ANGULAR RESPONSE OF PARAMETRIC ARRAYS—GENERAL NUMERICAL SOLUTION

M. ZHENG AND L.S. WANG

School of Electronic and Electrical Engineering, University of Birmingham, Edgbaston, B15 2TT, England

(*Received* 21 *January* 1999, *and in final form* 1 *June* 1999)

A numerical method is used to describe the angular amplitude and phase responses of non-saturation limited parametric arrays especially within the interaction region of the arrays. Farfield expression of the primary waves are employed in the method to approximate the primary fields. It is shown that the obtained numerical results are in close agreement with available experimental results both in farfield region and within the Rayleigh distance.

1. INTRODUCTION

A closed-form analytical solution is formulated to describe the farfield angular amplitude and phase responses of an absorption-limited parametric array in a previous paper [1]. Most practical parametric systems, however, work at such frequencies that most secondary signals are generated outside the Rayleigh distance. Moreover, some observation points are only a short distance away from the interaction region of a parametric array, or, on occasion, measurements can only be made within the interaction region due to some practical constraint. In all these cases, the analytical approach will not provide accurate predictions of the secondary fields. One solution to this problem is to numerically evaluate a three-dimensional integration which describes the secondary field for a given primary source. In this paper, a numerical solution is used to predict both angular amplitude and phase responses of parametric arrays not only in the farfield region, but also in the region well within the Rayleigh distance.

A number of authors have dealt with the three-dimensional integration for parametric arrays. Muir and Willette [2] employed a numerical integration approach to describe the pressure field of the sum and difference frequency in the far field of a circular piston source. Here the two primary waves are assumed to be spreading spherically from the source point and the position vector is treated with the exact law of cosine expression. It is straightforward to generalize the method to describe secondary field of any arbitrary source shape. Berktay and Leahy [3] presented a simplified three-dimensional integration which is more suitable for general farfield problems. Their results are expressed as normalized curves and a simplified equation which can be used for the design of farfield parametric arrays.

0022-460X/99/460177 + 21 $30.00/0

Fenlon [4] discussed a model based on the one-dimensional Burgers' equation and presented a quasi-plane three-dimensional equation that reduces to Burgers' equation in one dimension. This accounts for the diffraction effects due to spherically spreading primary waves, and he showed that the second order perturbation solution of this equation is in the form of a three-dimensional scattering integral similar to Westervelt's scattering integral. Moreover, a theoretical model that predicts the difference frequency pressure within the interaction region of a parametric array is given by Rolleigh [5]. Here, both linear and non-linear absorptions are neglected and it is assumed that the primary waves are spherically spreading throughout the interaction region. It is shown that with these assumptions the three-dimensional scattering integral can be reduced to a single integral if the primary pressure field is axially symmetrical. Mellen and Moffet made much more efforts to tackle the problem [6–10]. Mellen [6], firstly, introduced a numerical contour integration method to calculate the nearfield beam pattern of exponentially shaded end-fire-line arrays. Then he used the method to compute the nearfield axial secondary source levels of two exponentially shaded end-fire arrays of finite cross-section: a plane-collimated cylindrical array and a spherically divergent conical array [7]; and also calculate the nearfield beam pattern of continuous end-fire line arrays with an arbitrary amplitude shading [8]. In addition, Mellen and Moffet [9], presented the nearfield difference frequency waves in a triple integral which resulted from a transformation of the original integral to avoid the problem of a highly oscillating integrand. Later, the triple integral, applicable to saturation-limited as well as absorption-limited sources, was programmed for digital computation [10].

Although considerable research has been devoted to the evaluation of the three-dimensional integration both analytically and numerically, rather less attention has been paid to phase information (or arrival time) of the secondary waves in the solutions. Furthermore, the most favourable approach developed by Mellen and Moffet [9], employed a quite complicated transformation to obtain a new triple integral, which cannot readily be applied to different applications. Therefore, a straightforward numerical approach is used here to evaluate the three-dimensional integral which includes both amplitude and phase information.

Numerical solutions can provide good descriptions of the secondary field in the near field where there is considerable difference between analytic solutions and experimental results. For example, a parametric beamwidth narrower than Westervelt's theoretical prediction was frequently observed in many previous experiments by Bellin and Beyer [11], Hobæk [12], Zverov and Kalachev [13], Berktay and Smith [14], and Smith [15]. There are three possible causes of such a phenomenon. One explanation, put forward by Naze and Tjøtta [16] and Berktay [17], was that the "aperture effect" must be taken into consideration when estimating the directivity pattern of the difference frequency waves in which the interaction region is substantially limited to the near field of the projector by the rate of absorption of the primary waves. However, only some experimental results can be explained by the inclusion of this aperture factor, for example, Bellin and Beyer's experiment [11], while other results need further explanations. Smith's experimental results [15], showed that the measured difference frequency

beamwidth was narrower than the estimated value even if the aperture effect is included. The second explanation is that the observer is not sufficiently far from the interaction region. Berktay and Shooter [18], showed that the beam patterns within the nearfield region can be narrower than the farfield beam patterns. The final reason may be attributed to the amplitude and phase fluctuations within the Fresnel region of a projector as pointed out by Smith [15] and Moffett and Mellen [19]. However, no theoretical work has been carried to ascertain this because of the complicated nearfield characteristics. It remains unclear whether the fluctuations will make the difference frequency beam pattern broader or narrower.

In this paper, the parametric interaction process is treated in a quasi-linear manner, effects due to higher order interactions being neglected. Then the difference frequency source function is evaluated using Westervelt's treatment. Radiation from such sources is calculated as a scattering integral. A three-dimensional numerical integration is introduced for arbitrary spherically spreading primaries and both amplitude and phase information have been retained. Finally, a straightforward approach has been employed to perform the three-dimensional integration. The numerical solution is applied to a number of cases where experimental results are available. Very favourable results are obtained for all the cases.

2. THEORY

In the present analysis, all the assumptions of Westervelt's treatment are invoked. That is (1) the interaction occurs in a perfect fluid in which the effects of viscosity and heat conduction are neglected. However, the attenuation of the primary field is introduced in the *ad hoc* manner of Westervelt in order to avoid the on-axis singularity and (2) the fluid is homogeneous. Therefore, the secondary sound generated by a parametric array can be given by the following three-dimensional scattering integral,

$$p_s(\mathbf{R}, t) = \frac{\rho_0}{4\pi} \iiint \frac{(\partial/\partial t) q\,(t - \mathbf{r}/c_0)}{\mathbf{r}} \mathrm{d}V. \tag{1}$$

The scattering integral can be greatly simplified if it is assumed that the two primary waves are spherically spreading from the origin at angular frequencies of ω_1 and ω_2. These two primary waves can be expressed by

$$p_1(\mathbf{r}, t) = \frac{P_1 R_{01}}{r'} D_1(\varphi', \theta') \exp(-\alpha_1 r') \exp \mathrm{i}(\omega_1 t - k_1 r'), \tag{2}$$

$$p_2(\mathbf{r}, t) = \frac{P_2 R_{02}}{r'} D_2(\varphi', \theta') \exp(-\alpha_2 r') \exp \mathrm{i}(\omega_2 t - k_2 r'), \tag{3}$$

where $\mathbf{r}'$ is the distance vector from co-ordinate origin to source point, P_1, P_2 are the source pressures at the two primary frequencies 1 m from the centre of the source, R_{01}, R_{02} and α_1, α_2 are Rayleigh distance and absorption coefficient at primary

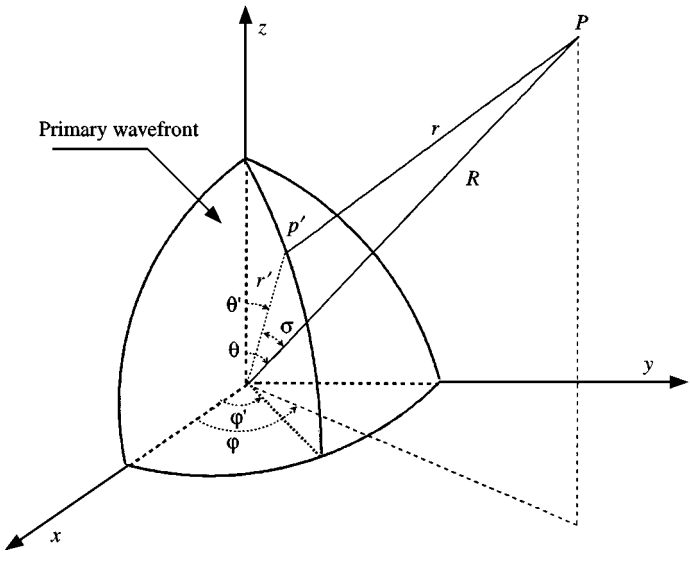

Figure 1. Geometry of spherical co-ordinates (P: Observation point; P': source point).

angular frequencies of ω_1 and ω_2, θ' and φ' are source point polar and azimuth angles, respectively, and $D_{1,2}(\theta, \varphi)$ is the normalized directivity function at the two primary frequencies. It should be pointed out that equations (2) and (3) describe only the far field of a source where the directivity function D is only a function of angles. The geometry is shown in Figure 1.

The source density function for the secondary wave at the difference frequency which results from interaction of the two primary waves, can be expressed by

$$q_{\omega_2-\omega_1} = \frac{-\beta(\omega_2-\omega_1)P_1P_2R_{01}R_{02}D_1D_2}{\rho_0^2c_0^4r'^2} \times \exp[-(\alpha_1+\alpha_2)r'] \exp i[(\omega_2-\omega_1)t-(k_2-k_1)r']. \tag{4}$$

Substituting equation (4) into equation (1), gives

$$P_d(R,\theta,\varphi,t) = -\frac{\beta P_1P_2R_{01}R_{02}(\omega_d)^2}{4\pi\rho_0^2c_0^4} \times \iiint_V \frac{D_1D_2\exp[-(\alpha_1+\alpha_2)r'-\alpha_d r]}{rr'^2} \exp i(\omega_d t - k_d r' - k_d r)\,dV, \tag{5}$$

where α_d is the absorption coefficient at the difference frequency. The modulus and argument of the complex integration represent the amplitude and phase responses of a parametric array respectively.

Finally, the integral in equation (5) is expressed in spherical polar co-ordinates

$$P_d(R,\theta,\varphi,t) = A_s \int_0^{\infty} \mathrm{d}r' \int_0^{\pi} \mathrm{d}\theta' \sin\theta' \int_0^{2\pi} \mathrm{d}\phi' F_s(r',\theta',\varphi',R,\theta,\varphi,t), \tag{6}$$

where

$$A_s = -\frac{\beta P_1 P_2 R_{01} R_{02} (\omega_d)^2}{4\pi\rho_0^2 c_0^4} \exp \mathrm{i}(\omega_d t), \tag{7}$$

$$F_s(r',\theta',\varphi',R,\theta,\varphi,t) = \frac{D_1(\theta',\varphi') D_2(\theta',\varphi') \exp[-(\alpha_1+\alpha_2) r' - \alpha_d r]}{r}$$

$$\times \exp[-\mathrm{i}(k_d r' + k_d r)], \tag{8}$$

$$r = \sqrt{R^2 + r'^2 - 2Rr'\cos\sigma}, \tag{9}$$

$$\cos\sigma = \frac{\mathbf{R}\cdot\mathbf{r}'}{|\mathbf{R}||\mathbf{r}'|} = \sin\theta\cos\varphi\sin\theta'\cos\varphi' + \sin\theta\sin\varphi\sin\theta'\sin\varphi' + \cos\varphi\cos\varphi'$$

$$= \sin\theta\sin\theta'\cos(\varphi-\varphi') + \cos\varphi\cos\varphi'. \tag{10}$$

Here r is the distance between source point and observation point, σ is the angle between source point vector $\mathbf{r}'$ and observation point vector $\mathbf{R}$.

The three-dimensional integration in equation (6) covers the whole space. In practice, the range of integration is taken only from the origin to the field point R. Since the scattering source decays exponentially, its contribution to the field point beyond R is negligible. Also, the upper limit on θ' integration is taken to an effective angle θ'_e covering the major concentration of primary wave radiation, namely to the angle of the first-side lobe.

It should be noted that the description of the primary waves by equations (2) and (3) are not accurate within the Rayleigh distance, where the primary fields resemble more plane waves than spherical waves. However, Rolleigh [5] proved that the error introduced by approximating these collimated plane waves by spherical waves inside the Rayleigh distance R_r at the primary frequency is negligible if the observation point is slightly beyond R_r.

The calculation of the three-dimensional integral is accomplished in the MATLAB environment. The first integration is performed by using MATLAB's intrinsic function TRAPZ where the trapezoidal method is used. There are more advanced methods such as QUAD, using adaptive recursive Simpson's rule and QUAD8, using adaptive recursive Newton Cotes 8 panel rule, in MATLAB. However, when there is a highly oscillating integrand, tests indicate that the trapezoidal method has a much better performance than either adaptive recursive Simpson's routine or adaptive recursive Newton Cotes 8 panel procedure. Thus, the trapezoidal method has been chosen for the first integration. For the second and third integrations, the Simpson's rule [20] is applied. It is found that the suggested method for the three-dimensional numerical integration has good convergence.

3. EXPERIMENTAL AND NUMERICAL RESULTS

Rolleigh [21] pointed out that there were controversial results concerning the difference frequency beamwidth of parametric arrays. For instance, Rolleigh's results show a decrease in difference frequency beamwidth as the observation distance increases. Berkaty's results [22], however, indicated that the difference frequency beamwidth increased with an increasing measurement range. Rolleigh attributed this "discrepancy" to a limitation of the Berktay model which is valid only when the observation point is outside the interaction region.

In order to reconcile the results, the angular responses at different ranges were investigated for both absorption-limited and spreading-loss-limited parametric arrays using the numerical approach. The results are compared with experimental data to demonstrate the capability of the numerical method.

3.1. Case 1

Some preliminary experiments were performed in a laboratory tank [1]. A circular transducer with a 30 mm diameter and a resonance frequency of 2·54 MHz, was employed, which was mounted on a tilt mechanism to allow angle adjustment in the vertical plane. The observation distance is 7·8 m away from the transducer. The acoustic power was kept at a maximum signal-to-noise ratio but below the saturation limit [23]. The angular amplitude and phase responses are measured at two secondary frequencies, 270 and 410 kHz.

Figures 2 and 3 show the measured secondary wave as a function of time and angle with respect to the axis at 270 and 410 kHz respectively. One can see from these figures that, in addition to the expected reduction in amplitude there is a time delay in the secondary signal when observation point is away from the axis.

It is interesting to compare the experimental results with the theoretical results given by the analytical solution given in reference [1]. Figures 4 and 5 show the corresponding analytical results. One can observe clearly that there is a greater off-axis phase delay in the theoretical results in comparison with that of the experimental results. For a better comparison, individual relative amplitudes and phase shifts at different off-axis angles are also shown in Figures 6 and 7 respectively.

It can be seen that there are some discrepancies between the experimental and analytical results both for amplitudes and phases. For the phase shifts, as the off-axis angle increases, more disagreements between experimental and analytical results occur. For amplitude responses, analytical curves have a more flat appearance at small off-axis angles, by comparison with the experimental curves which exhibit almost triangular shapes. This phenomenon was also observed by Moffet and Mellen [19] at a large down-shift ratio. The reason for these discrepancies may be attributed to two reasons. Firstly, in the present parametric transduction the length of the virtual array $R_v = 1/2\alpha_0 = 2{\cdot}8$ m, and the Rayleigh distance $R_r = S/\lambda_c = \pi a^2 f_c/c_0 = 1{\cdot}2$ m. Therefore, $R_v > R_r$ and their values are not comparably close. Apparently, this is a spreading-loss-limited parametric array, therefore the analytical solution, only suitable for absorption-limited arrays, are not applicable. Secondly, the

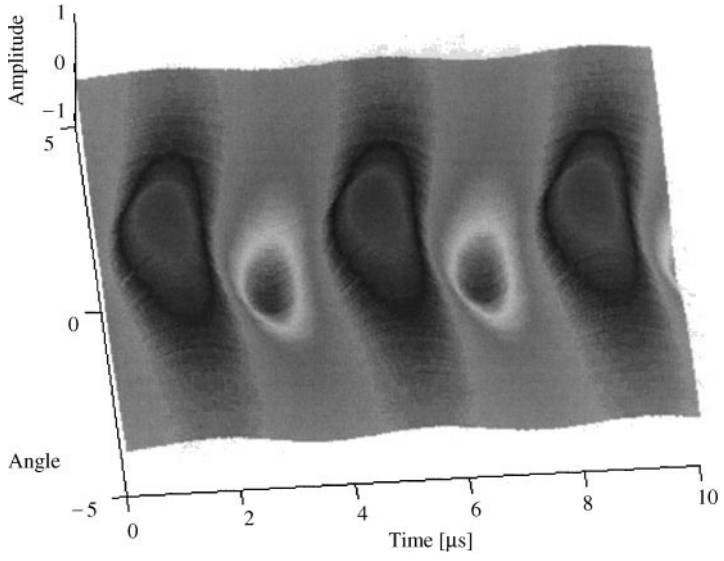

Figure 2. Parametric off-axis experimental result ($f_c = 2{\cdot}54$ MHz, $f_d = 270$ kHz).

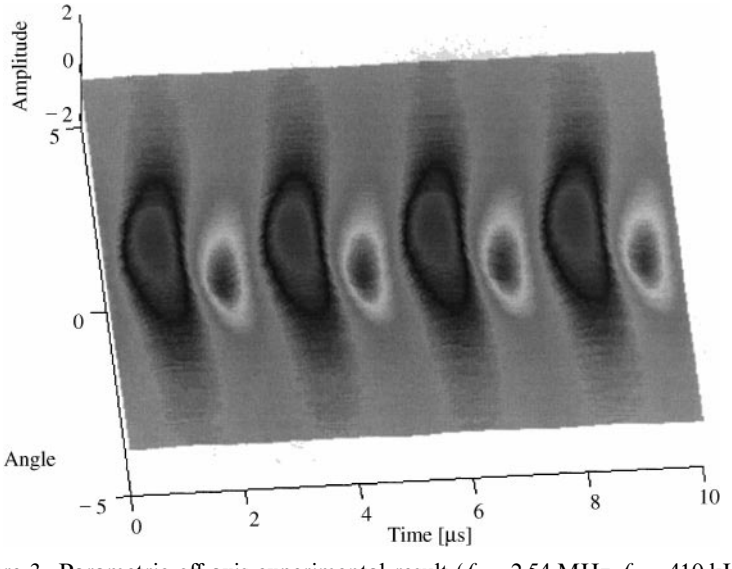

Figure 3. Parametric off-axis experimental result ($f_c = 2{\cdot}54$ MHz, $f_d = 410$ kHz).

measurement distance R_m is only 7·8 m away from the primary transducer, so the assumption of $R_m \gg R_v$, which is used to achieve analytical results, cannot be sufficiently satisfied.

To solve the above problem, the three-dimensional integral in equation (6) has been evaluated numerically for this case. The sound pressure at the primary frequencies was selected to produce an acoustic power just less than 10 W to avoid saturation. The normalized results are shown in Figures 6 and 7. It can be seen that

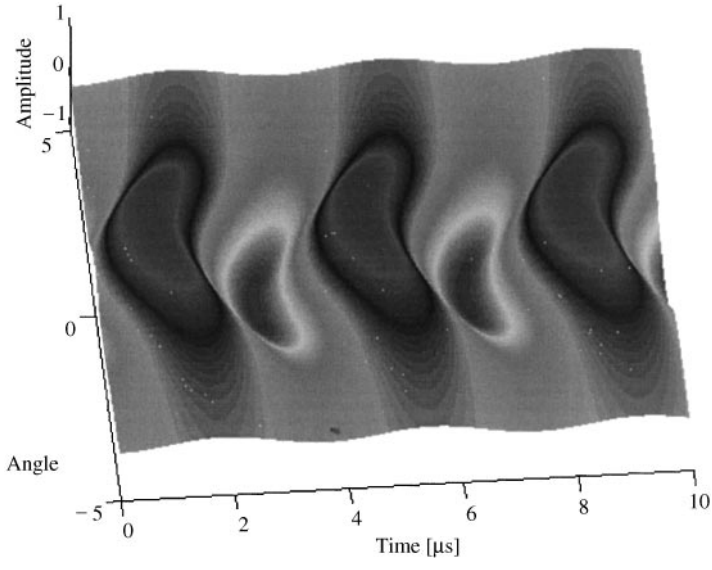

Figure 4. Parametric off-axis analytical result ($f_c = 2{\cdot}54$ MHz, $f_d = 270$ kHz).

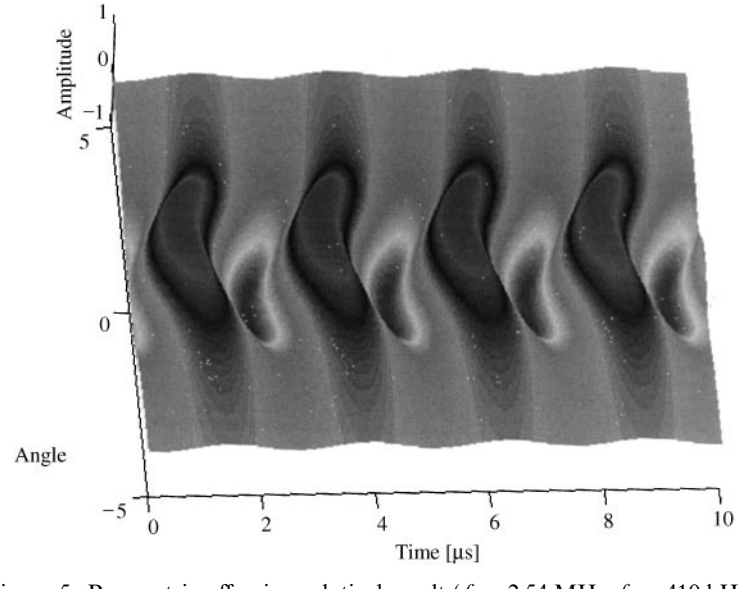

Figure 5. Parametric off-axis analytical result ($f_c = 2{\cdot}54$ MHz, $f_d = 410$ kHz).

there are good agreements between the numerical results and the experimental data for both amplitudes and phases at frequencies of 270 and 410 kHz respectively.

3.2. Case 2

The parametric transduction process became absorption-limited when the primary frequency was doubled with the same experimental set-up in the previous case. The

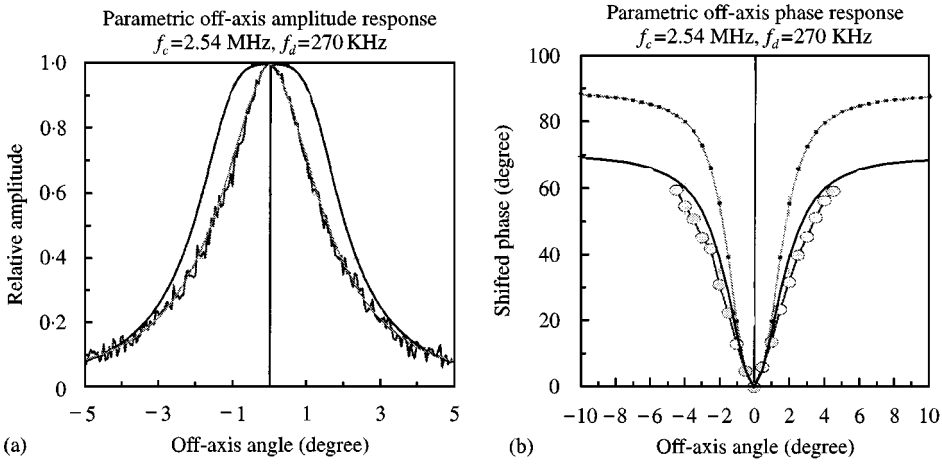

Figure 6. Angular amplitude and phase responses at 7·8 m from the source at 270 kHz. (a) —, Analytic; —, Experiment; ····· , 3D-numeric. (b) –•– , Analytic; –○– , Experiment; —, 3-D numeric.

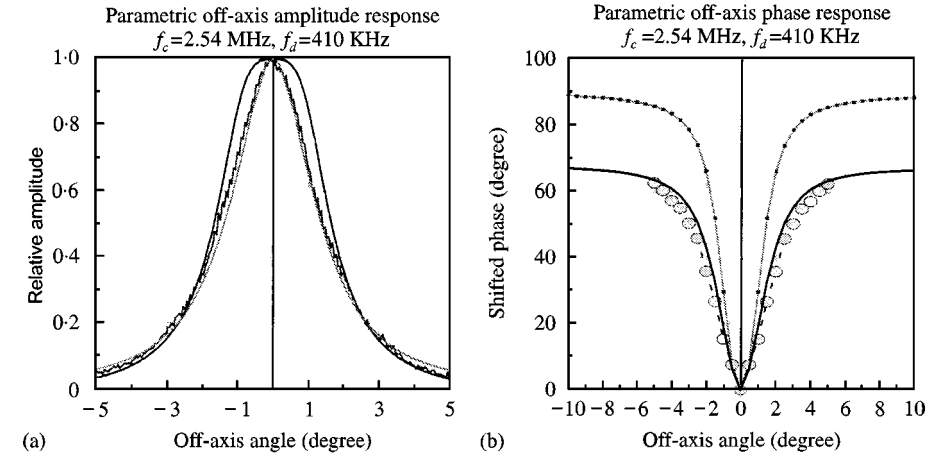

Figure 7. Angular amplitude and phase responses at 7·8 m from the source at 410 kHz. (a) —, Analytic; —, Experiment; ····· , 3-D numeric. (b) –•– , Analytic; –○– , Experiment; —, 3-D numeric.

experimental results of angular amplitude and phase responses in this case are presented in Figures 8 and 9 for a primary frequency of 6·2 MHz and a difference frequency of 270 kHz at ranges of 0·4, 1·5 and 7·5 m respectively. In Figures 8 and 9, numerical reults are also plotted. It can be seen that there are good agreements between numerical integration results and experimental data, especially at the range of 7·5 m where excellent agreements are achieved.

It is shown in Figure 8 that, for the amplitude response, the beam pattern becomes narrower as the observation distance is getting closer to the projector. This trend can be seen in Figure 10 as well. For example, the 3 dB beamwidth is about 7° at 7·5 m, and only 2·7° at 0·4 m, which is just above one-third of the beamwidth of the former. Moreover, if the measurement point is moved closer to the projector, then there is

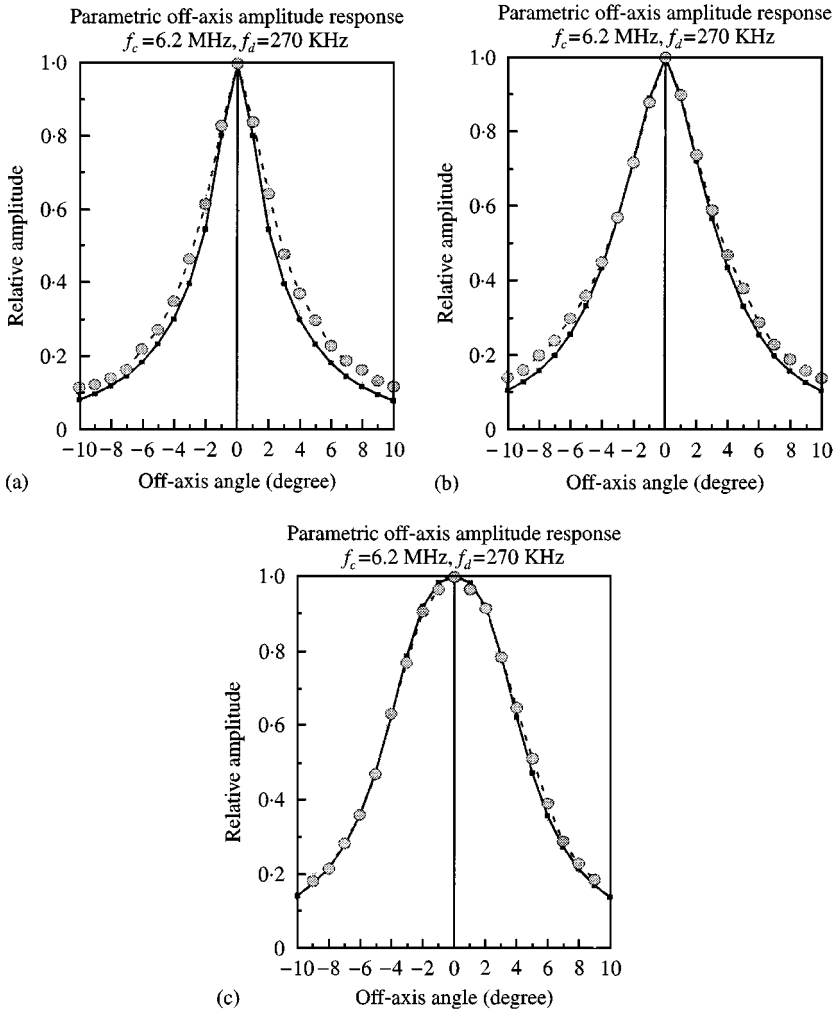

Figure 8. Parametric angular amplitude responses (a) —▪— , 3-D numeric; —○— , Exp 0·4 m. (b) —▪— , 3-D numeric; —○— , Exp 1·5 m. (c) —▪— , 3-D numeric; —○— , Exp 7·5 m.

a range below which the beamwidth of the difference frequency increases. This 3-D numerical result confirms Vestrheim and Hobæk's experimental result [24]. In their experiment, the two primary waves with frequencies of 17·68 and 16·68 MHz are radiated from a planar, circular quartz source with an effective radius of 6·5 mm. They observed a minimum beamwidth at about 20 cm from the projector.

From Figure 9, it can be seen that the off-axis phase shift increases slightly with the observation distances.

The phenomenon of a narrowing beam pattern at shorter ranges, was also observed by Merklinger [25], but no explanation was given in his thesis. Later, Berktay [22], tried to explain this phenomenon by using a second order approximation for the range vector between the scattering and observation points. It appears that, at reasonably long ranges within the near field, Berktay's theory can explain the

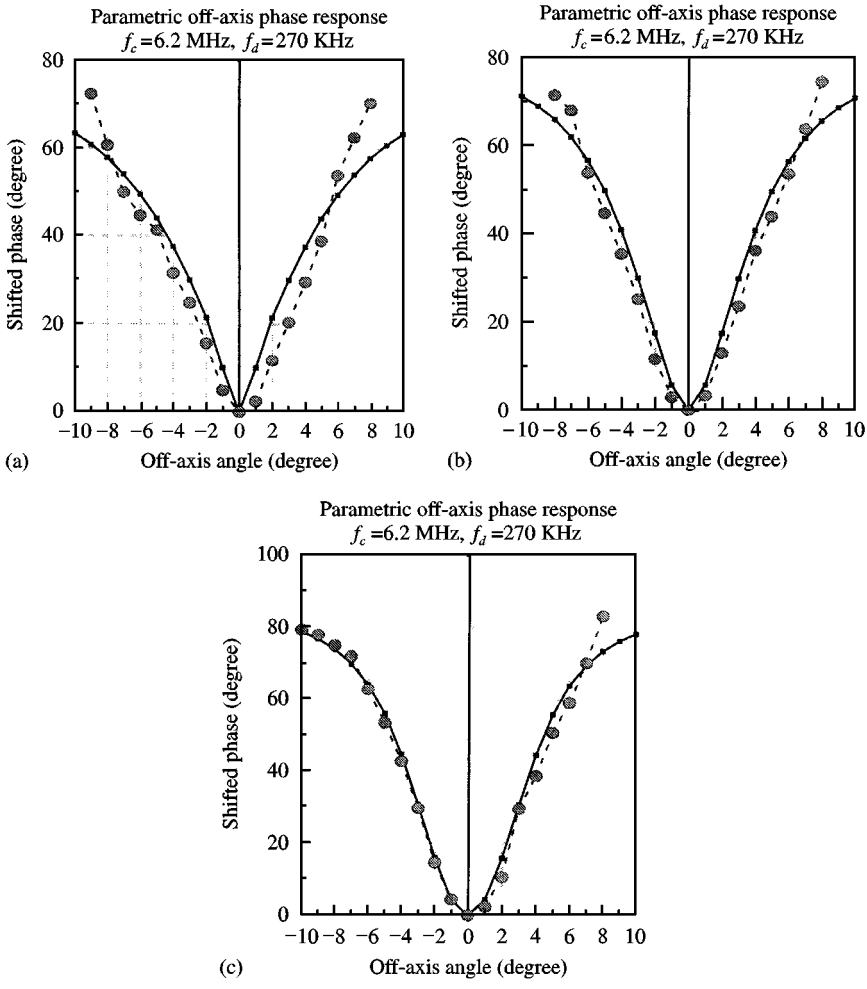

Figure 9. Parametric angular phase responses (a) —■—, 3-D numeric; —○—, Exp 0·4 m. (b) —■—, 3-D numeric; —○—, Exp 1·5 m. (c) —■—, 3-D numeric; —○—, Exp 7·5 m.

narrower beam pattern phenomenon. For example, in Merklinger's case, at a range of 1·7 m for a source with a primary frequency centred at 8·75 MHz and a difference frequency of 1·1 MHz and also Smith's case [15], at a range of 5 m for a source with a primary frequency of 3 MHz and difference frequencies between 100 and 500 kHz. However, at much shorter ranges, his theory does not explain the rapid narrowing of the beams.

Here, an attempt is made to solve the above problem by use of three-dimensional numerical integration. The integral is applied to Merklinger's case, where a 1 cm square transducer was used to generate a centre primary frequency of 8·75 MHz and a difference frequency of 1·1 MHz, the parametric array has Rayleigh distance $R_r = 0{\cdot}58$ m and virtual array distance $R_v = 0{\cdot}27$ m. The beam pattern at different ranges is compared with the numerical prediction in Figure 11. The 3 dB beam width of the parametric array is plotted against the numerical result in Figure 12. It can be

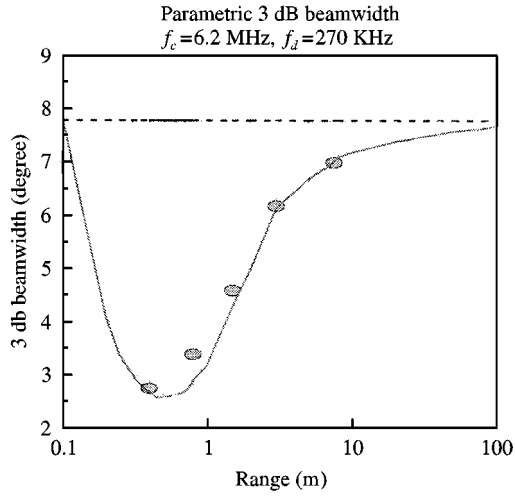

Figure 10. Parametric 3 dB beamwidth at different ranges ($f_c = 6{\cdot}2$ MHz, $f_d = 270$ kHz). (a) – – –, Analytic; ⟲, Exp; ····, 3D-numeric.

clearly seen that there are good agreements between the 3-D numerical results and the experimental results, even for the very short ranges such as 0·25 and 0·625 m. This again confirms the validity of the three-dimensional integral solution.

One may conclude that when observation ranges decrease, the beam patterns of absorption-limited arrays become narrower. However, at very close vicinity of a parametric source, there is a minimum beamwidth range within which the beam width, on the contrary, increases.

3.3. Case 3

To further check the phase shifts of parametric arrays, a lower frequency parametric array was investigated in a quarry at Tamworth, England. A transducer, 150 mm × 150 mm square piezoelectric ceramic plate with a 300 kHz thickness mode resonant frequency, was used to generate primary waves. In this experiment, the transducer was fixed in a pan and tilt system which is capable of rotating the array by $\pm 10^\circ$ in the vertical plane and $\pm 30^\circ$ in the horizontal plane. The pan and tilt unit was driven by stepper motors which were remotely operated via a personal computer. A compass and inclinometer, attached to the transducer mounting frame were employed to monitor the orientation of the transmit transducer.

To measure the phase shift, a primary centre frequency of 315 kHz and difference frequency of 50 kHz were used. Measurements were performed over a range of 125 m. From the parameters provided, the parametric array has virtual array distance $R_v = 163$ m and a Rayleigh distance $R_r = 5{\cdot}0$ m, since $R_v \gg R_r$, the source strictly belongs to a spreading-loss-limited parametric array. Consequently, the analytical closed-form formula cannot be applied to this case.

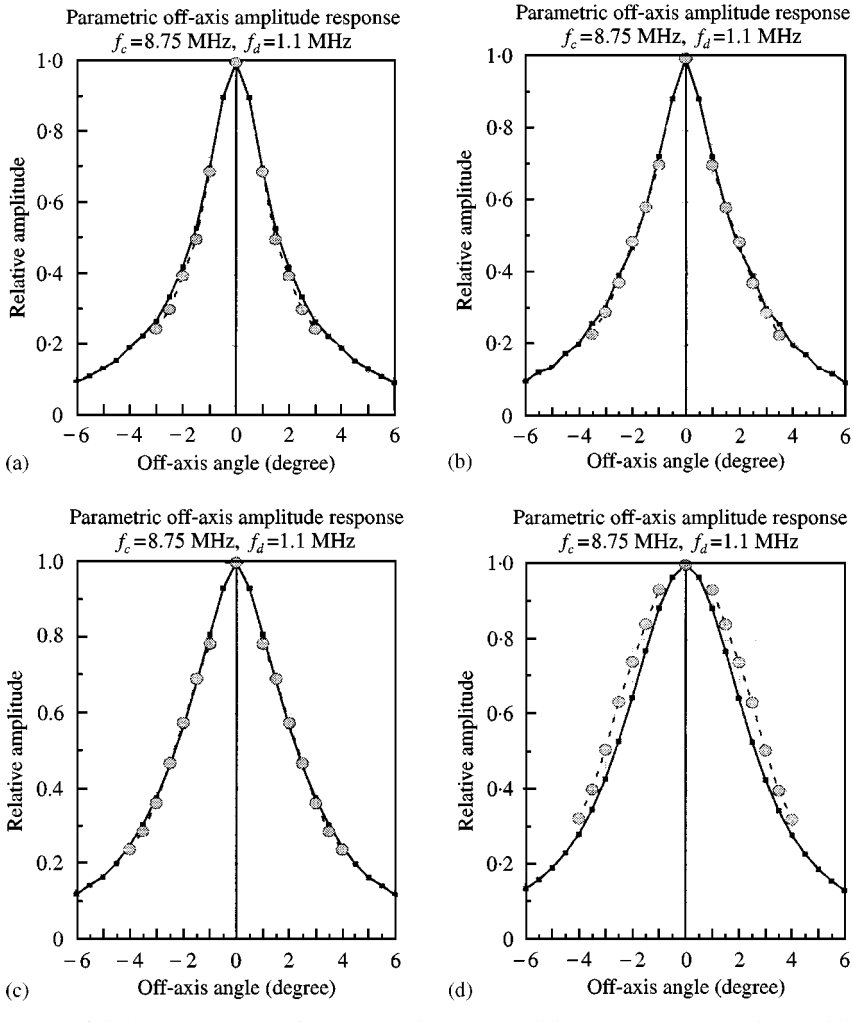

Figure 11. Nearfield beam patterns of a parametric array at different ranges (Experimental data from Merklinger [25]). (a) —▪—, 3-D numeric (spheric); —○—, Exp (0·25 m). (b) —▪—, 3-D numeric (spheric); —○—, Exp (0·625 m). (c) —▪—, 3-D numeric (spheric); —○—, Exp (1 m). (d) —▪—, 3-D numeric (spheric); —○—, Exp (1·5 m).

For comparison purposes, the experimental results as well as the numerical results for amplitude and phase responses at ranges of 7 and 125 m are shown in Figures 13 and 14 respectively.

It should be pointed out that there is a small side lobe at a positive angle in Figure 14. This is because of the interference of the surface reflected multi-path at a large off-axis angle. A simple geometric calculation confirmed the existence of the surface reflected multi-path.

From Figures 13 and 14 it can be observed that the numerical results agree well with the experimental data both for amplitude and phase responses. The 3 dB beamwidth versus range is shown in Figure 15, which, again, offers a good agreement between the measured and predicted results.

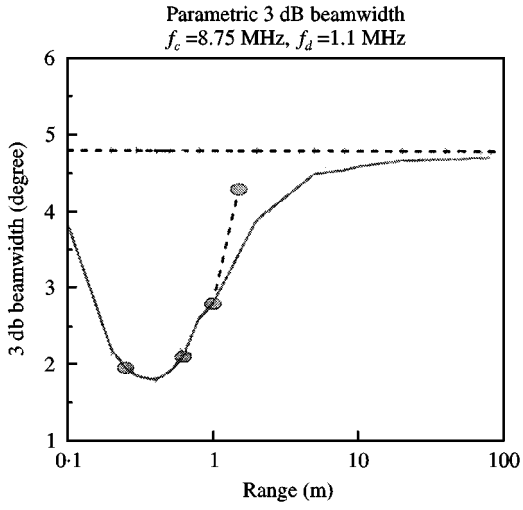

Figure 12. 3 dB beamwidth of the parametric array at different ranges (Experimental data from Merklinger [25]). – – –, Analytic; ⟲, Exp; ·····, 3-D numeric.

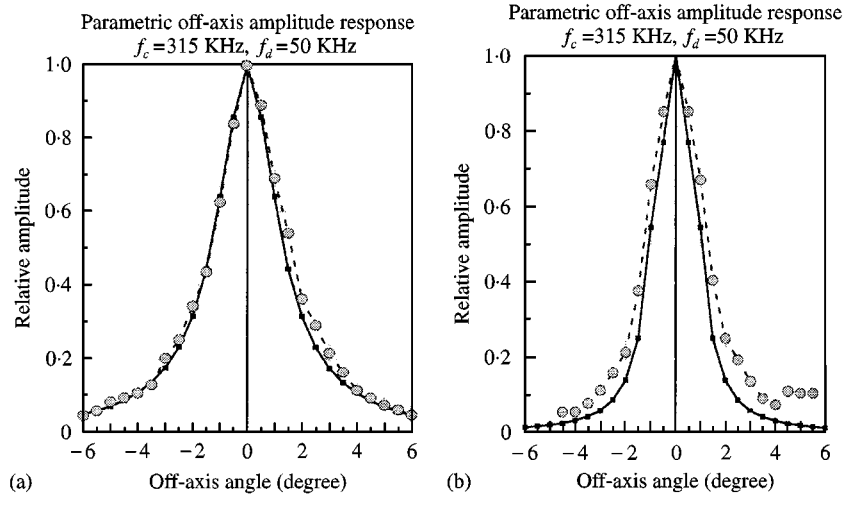

Figure 13. Comparison between experimental and 3-D numerical results of amplitude response (a) ▬■▬, Num (7 m); ⟲, Exp (7 m). (b) ▬■▬, Num (125 m); ⟲, Exp (125 m).

To illustrate the method further, the frequently cited experimental data given by Muir and Willette [2], which has not been theoretically analyzed, have also been compared with the 3-D numerical integration results,. In their experiment, a 3-in.-diameter piston projector was used to generate a centre primary frequency of 450 kHz and a difference frequency of 64 kHz in a fresh-water lake. The 3 dB beamwidths at different ranges are shown in Figure 16, from which it can be seen that there is, in general, a good agreement between the numerical and experimental

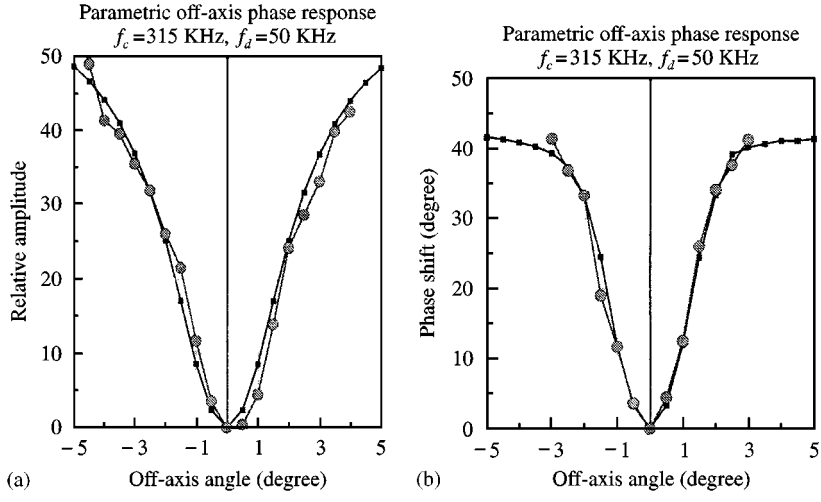

Figure 14. Comparison between experimental and 3-D numerical results of phase response (a) —■—, Num (7 m); —○—, Exp (7 m). (b) —■—, Num (125 m); —○—, Exp (125 m).

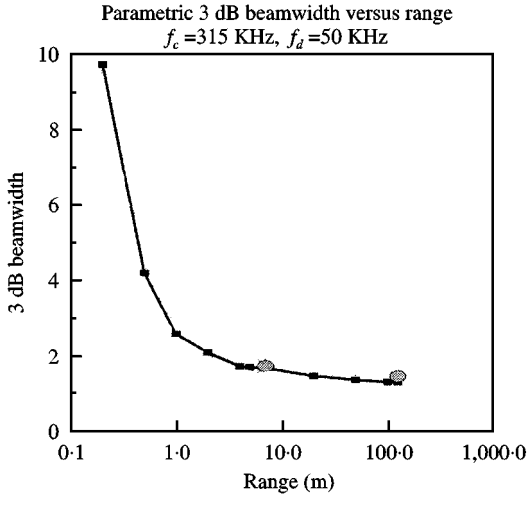

Figure 15. 3-dB beamwidth at different ranges. —■—, 3-D numeric; —○—, Experiment.

results. It can also be seen that as the measurement range decreases the beam width becomes wider. Furthermore, as the observation point is very close to the projector, the beamwidth will be much wider than that would be expected in the far field.

It is worth noticing that spreading-loss-limited parametric arrays develop their narrow beam feature early in the interaction process. At ranges just beyond the Rayleigh distance the beamwidth almost reaches the farfield value. The reason for this may be attributed to the exponentially shading characteristics of the parametric scattering sources. Their nearfield beamwidths, therefore, approach the farfield value with an exponential range dependence.

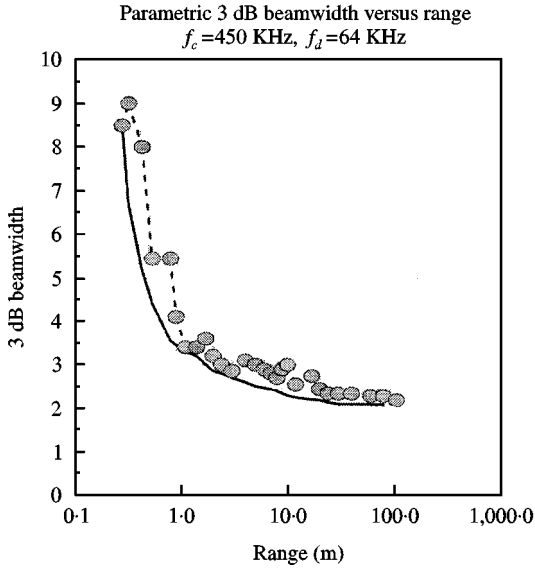

Figure 16. 3-dB beamwidth at different ranges. ····· , 3-D numeric; -o- , Experiment.

4. EVALUATION OF THE APPROXIMATIONS USED IN ANALYTIC SOLUTIONS FOR PARAMETRIC ARRAYS

In order to obtain closed-form solutions to parametric arrays, some approximations have to be made to the position vector **r**. The exact equation for the position vector **r** is presented in equation (9). The most frequently used approximations are the first and the second order approximations by Westervelt and Berktay. In Westervelt's approximation [26], the position vector **r** is simplified by

$$r = R - r' \cos \sigma, \tag{11}$$

while in Berktay's approximation [22], the position vector **r** is expressed by

$$r = R - r' \cos \sigma + (r'^2/2R) \sin^2 \sigma. \tag{12}$$

It is interesting to examine the effects of these two approximations against the exact expression in the three-dimensional integral with the numerical method in section 2.

The first case to be examined is the parametric array discussed in section 3.2. This array has a primary frequency of 6·2 MHz and a difference frequency of 270 kHz. The numerical results of angular amplitude responses for different approaches as well as experimental results are shown in Figure 17 at ranges of 0·4, 1·5 and 7·5 m respectively. Figure 18 also shows the 3 dB beamwidth for the different methods as well as experimental results.

From Figures 17 and 18, it can be seen that at a long range which is about 10 times of virtual array distance both Westervelt and Berktay approximations lead to a good

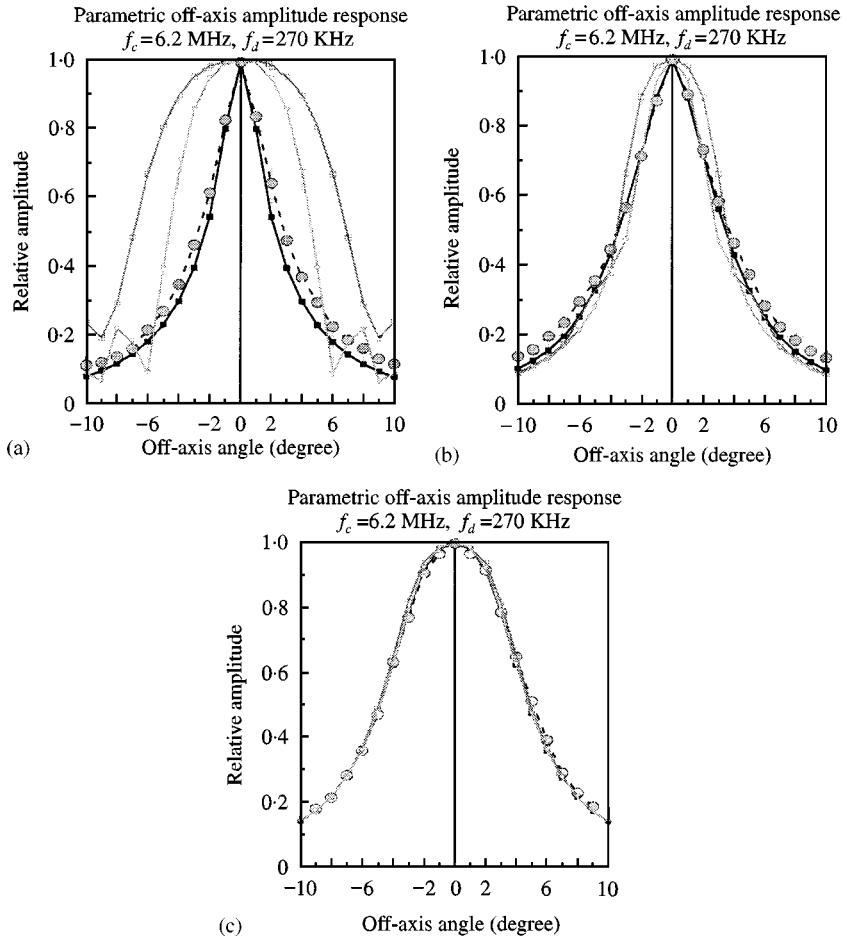

Figure 17. Parametric angular amplitude responses (a: 0·4 m, b: 1·5 m, c: 7·5 m). (a) —■—, 3-D numeric; —○—, Exp 0·4 m; —•—, 3-D (Westervelt approx.); ···, 3-D (Berktay approx.). (b) —■—, 3-D numeric; —○—, Exp 1·5 m; ···, 3-D (Westervelt approx.); ···, 3-D (Berktay approx.). (c) —■—, 3-D numeric; —○—, Exp 7·5 m; —•—, 3-D (Westervelt approx.); ···, 3-D (Berktay approx.).

agreement with 3-D numerical integration of the exact position vector or experimental results. Here the virtual array distance $R_v = 0{\cdot}46$ m. As the observation distance decreases, the Berktay's approximation provides better results than that of Westervelt's, but it still exhibits some discrepancies from the experimental results and the exact numerical solution. That is, the predicted beam patterns using Westervelt and Berktay's approximations are wider than those measured. When observation points are closer to the projector, more errors are introduced.

It should be stated that the above comparison results show us the limitation of Berktay's theoretical approach in dealing with the rapid narrowing of beams at shorter ranges in Merklinger's experiment [25]. This can be further confirmed by checking Merklinger's case, where a centre primary frequency of 8·75 MHz was used to generate a difference frequency of 1·1 MHz. The numerical results using different

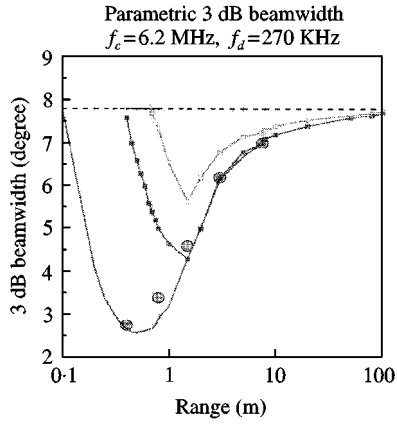

Figure 18. 3-dB beamwidth at different ranges. – – –, Analytic; ○, Exp; —, 3-D numeric; ✱, Westervelt approx.; ■, Berktay approx. ⋯).

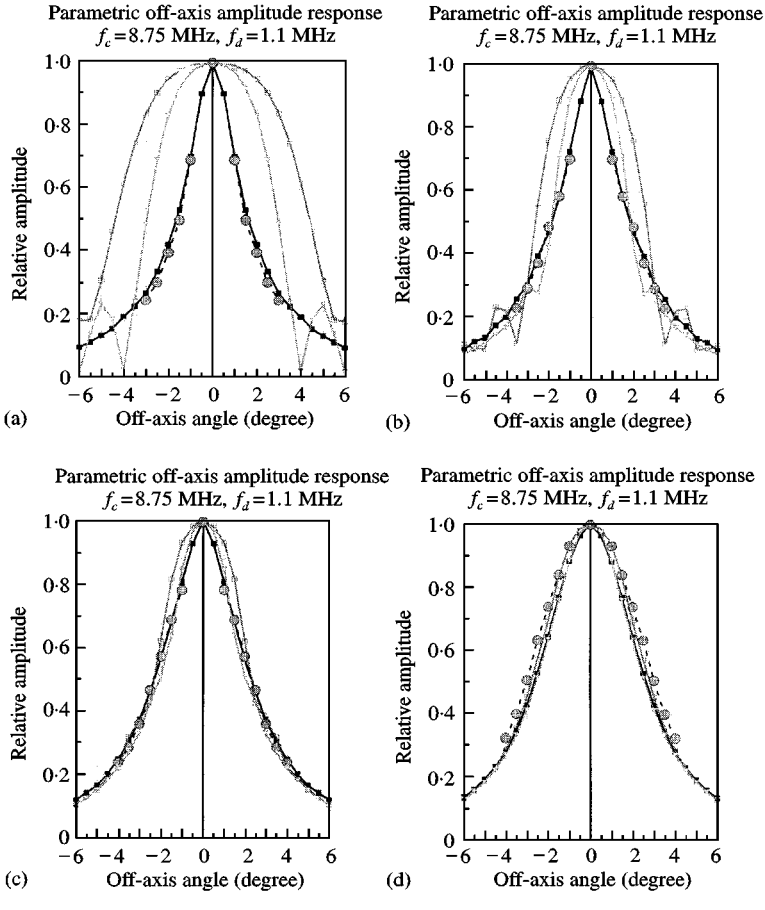

Figure 19. Parametric nearfield beam patterns, (a) ■, 3-D numeric; ○, Exp 0·25 m; ■, 3-D (Westervelt approx.); ✱, 3-D (Berktay approx.). (b) ■, 3-D numeric; ○, Exp 0·625 m; ■, 3-D (Westervelt approx.); ✱, 3-D (Berktay approx.). (c) ■, 3-D numeric; ○, Exp 1 m; ■, 3-D (Westervelt approx.); ✱, 3-D (Berktay approx.). (d) ■, 3-D numeric; ○, Exp 1·5 m; ■, 3-D (Westervelt approx.); ✱, 3-D (Berktay approx.).

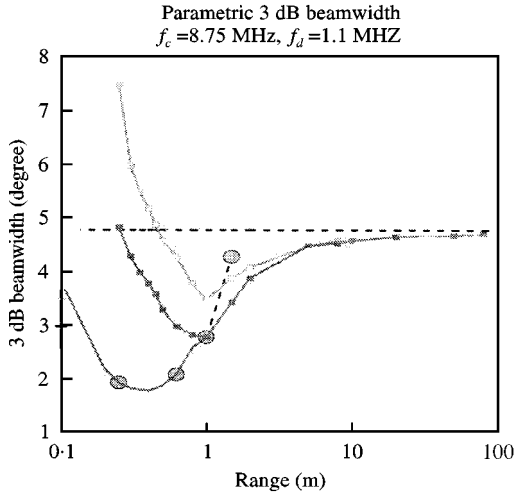

Figure 20. 3 dB beamwidth at different ranges. – – –, Analytic; ⟲, Exp; ····, 3-D numeric; –•–, Westervelt approx.; –•–, Berktay approx.).

vectors as well as experimental results are shown in Figure 19 at ranges of 0·25, 0·625, 1 and 1·5 m respectively. The 3 dB beamwidth of difference frequency is also presented in Figure 20.

From Figure 20, it can be observed that at a range of 1·7 m Berktay's approximation provides good agreement with the experimental data as well as the 3-D numerical integration results. At a range of 1 m Berktay's approximation shows a slight departure from the experimental data and at a range of 0·625 m more deviation is exhibited.

Clearly, it is the exact position vector solution, rather than Berktay's approximation, that provides a good prediction of amplitude angular responses both in the far and near field of absorption-limited parametric arrays. Only at some distance from the interaction region Berktay's or Westervelt's approximations can be used to predict angular amplitude responses.

5. CONCLUSIONS

A numerical method for the secondary field as a three-dimensional integral has been developed and used to provide accurate evaluations on the angular amplitude and phase responses of non-saturation-limited parametric arrays both in near and farfield regions. The experiments and numerical predictions have shown that, for absorption-limited parametric arrays in the far field, the beamwidth at the difference frequency reduces when the measurement range decreases. As the observation point moves closer to the projector, there is a range at which a minimum beamwidth is achieved, below this range the beamwidth increases again. However, for spreading-loss-limited parametric arrays, as the observation distance decreases, the beamwidth of the difference frequency monotonically increases. Further examination of the frequently used position vectors revealed that, the failure to explain the rapid

narrowing of the beam at shorter ranges for absorption-limited parametric arrays is due to the approximations which are not suitable for the very near field.

ACKNOWLEDGMENTS

The authors are grateful for the assistance of Mr Richard Stoner in the field trials. This work is sponsored by EEC contract MAST2-CT91005.

REFERENCES

1. M. Zheng and R. F. W. Coates 1998 *Journal of Sound and Vibration* **209**, 493–503. The angular response of a parametric array: analytical solution.
2. T. G. Muir and J. G. Willette 1972 *Journal of the Acoustical Society of America* **52**, 1481–1486. Parametric acoustic transmitting arrays.
3. H. O. Berktay and D. J. Leahy 1974 *Journal of the Acoustical Society of America* **55**, 539–546. Farfield performance of parametric transmitters.
4. F. H. Fenlon 1974 *Journal of the Acoustical Society of America* **55**, 35–46. On the performance of a dual frequency parametric source via matched asymptotic solution of Burgers' equation.
5. R. L. Rolleigh 1975 *Journal of the Acoustical Society of America* **58**, 964–971. Difference frequency pressure within the interaction region of a parametric array.
6. R. H. Mellen 1976 *Journal of the Acoustical Society of America* **61**, 599–602. Nearfield axial level of exponentially shaded end-fire array.
7. R. H. Mellen 1977 *Journal of the Acoustical Society of America* **61**, 505–506. Nearfield beam pattern of exponentially shaded end-fire line arrays.
8. R. H. Mellen 1976 *Journal of the Acoustical Society of America* **61**, 883–884. Nearfield beam pattern of end-fire line arrays with arbitrary shading.
9. R. H. Mellen and M. B. Moffet 1978 *Journal of the Acoustical Society of America* **63**, 1622–1624. A numeric method for calculating the nearfield of a parametric acoustic source.
10. M. B. Moffet and R. H. Mellen 1981 *Journal of the Acoustical Society of America* **69**, 404–409. Nearfield characteristics of parametric acoustic source.
11. J. L. S. Bellin and R. T. Beyer 1962 *Journal of the Acoustical Society of America* **34**, 1051–1054. Experimental investigation of end-fire array.
12. H. Hobæk 1967 *Journal of the Sound and Vibration* **6**, 460–463. Experimental investigation of an acoustical end-fire array.
13. V. A. Zverev and A. I. Kalachev 1968 *Soviet Physics and Acoustics* **14**, 173–178. Measurement of the scattering of sound in the superposition of parallel beams.
14. H. O. Berktay and B. V. Smith 1965 *Electronic Letters* **1**, End-fire array of virtual sound sources arising from the interaction of sound waves.
15. B. V. Smith 1971 *Journal of Sound and Vibration* **14**, 7–21. An experimental study of a parametric end-fire array.
16. J. Naze and S. Tjøtta 1965 *Journal of the Acoustical Society of America* **37**, 174–175. Nonlinear interaction of two sound beams.
17. H. O. Berktay 1965 *Journal of Sound and Vibration* **2**, 435–461. Possible exploitation of non-linear acoustics in the underwater transmitting applications.
18. H. O. Berktay and J. A. Shooter 1973 *Journal of the Acoustical Society of America* **53**, 550–556. Nearfield effects in end-fire line array.
19. M. B. Moffet and R. H. Mellen 1977 *Journal of the Acoustical Society of America* **61**, 325–337. Model for parametric acoustic source.
20. G. R. Lindfield and J. E. Penny 1989 *Microcomputers in Numerical Analysis.* Chichester, UK: Ellis Horwood.

21. R. L. Rolleigh 1975 *Journal of the Acoustical Society of America* **58**, 964–971. Difference frequency pressure within the interaction region of a parametric array.
22. H. O. Berktay 1972 *Journal of Sound and Vibration* **20**, 135–143. Near-field effects in parametric end-fire arrays.
23. M. Zheng 1996 *Ph. D. thesis*, *The University of Birmingham*. Underwater acoustic communications utilising parametric transduction with M-ary differential phase-shift keying.
24. M. Vestrheim and H. Hobæk 1971 *Proceeding of Symposium on Nonlinear Acoustics* Held at The University of Birmingham on 1st and 2nd April, 159–169. Angular distribution of nonlinearly generated difference frequency sound.
25. H. M. Merklinger 1971 *Ph. D. thesis*, *The University of Birmingham*. High intensity effects in the non-linear acoustic parametric end-fire array.
26. P. J. Westervelt 1963 *Journal of the Acoustical Society of America* **35**, 535–537. Parametric acoustic array.